J Nanostruct 13(4): 1050-1065, Autumn 2023

RESEARCH PAPER

# Removal of Bromocresol Green by Nanocomposite Based on Chitosan/$Nb_2O_5$/$MnO_2$ and Chitosan /$Nb_2O_5$/$Cr_2O_3$

*Karrar M. Obaid *, Ahmed S. Abbas, Yahya F. Al-Khafaji*

*Chemistry Department, College of Science, Babylon University, Hilla, Iraq*

ARTICLE INFO

***Article History:***
*Received 11 July 2023*
*Accepted 25 September 2023*
*Published 01 October 2023*

***Keywords:***
*Adsorption*
*Bi-metal oxide*
*Bromocresol green*
*Chitosan*
*Dye Removal*

ABSTRACT

Chitosan poly(methacrylate) composites were created and used in the current investigation to adsorb bromocresol green from aqueous solutions. a new type of multifunctional material Chitosan/$Nb_2O_5$/$MnO_2$ and Chitosan /$Nb_2O_5$/$Cr_2O_3$ nanocomposite was prepared by situ chemistry approach. The composites that were created were identified by thermogravimetric analysis, X-ray diffraction, scanning electron microscopy, and Fourier transform infrared spectroscopy. The impacts of experimental factors, including sample pH and adsorption period, were also looked at in relation to the bromocresol green elimination by the proposed adsorbent. Additionally, a thorough examination of the adsorption properties of the synthesized adsorbent, including kinetics, adsorption isotherms, and thermodynamics, was conducted. The Freundlich model accurately predicted the adsorption isotherm, and after 10 minutes of shaking at pH 7.0 and pH10, the maximum adsorption capacity was determined to be (604,166) g mg-1.for Chitosan/$Nb_2O_5$/$MnO_2$ and Chitosan /$Nb_2O_5$/$Cr_2O_3$ respectively.

**How to cite this article**
*Obaid K., Abbas A., Al-Khafaji Y. Aadorption,Removal of Bromocresol Green by Nanocomposite Based on Chitosan/$Nb_2O_5$/$MnO_2$ and Chitosan /$Nb_2O_5$/$Cr_2O_3$. J Nanostruct, 2023; 13(4):1050-1065. DOI: 10.22052/JNS.2023.04.014*

## INTRODUCTION

For a very long time, the textile industry's main issue has been wastewater treatment. These effluents contain different synthetic materials, including dyestuffs. There are more than 100,000 commercially accessible dyes, and more than 700,000 tones are created yearly. Synthetic dyes are common water contaminants because of their high solubility, and they are frequently present in trace amounts in industrial wastewater [1,2]. The majority of dye wastewater that is released into the environment comes from the textile sector (54%) and accounts for more than half of all dye effluents that are now found in the environment. Examples of such dyes are Bromocresol green (BCG) [3]. The public's perception of water quality is significantly influenced by color, and the presence of even very minute amounts of dyes is highly evident. As a result, there are more and more concerns and worries. The critical ecological issue of environmental dye contamination is exacerbated by the fact that the majority of dyes are challenging to break down utilizing conventional biological processes. Additionally, during the past two decades, there have been worries about the possible toxicity of dyes and their precursors, which constitute a major risk to aquatic living things [4,5]. Techniques including flocculation and coagulation [6], ozonation [6], adsorption [7], electrochemical [8] and fungal decolonization [9]

* *Corresponding Author Email: karrar.majeed1993@gmail.com*

as well as physiochemical, biological, and chemical methods, are new developments in color removal technology. Adsorption has become more popular among these techniques because it is effective and economical at removing colors from effluents.[10] A substance (an ion, atom, or molecule) from its liquid or gaseous surroundings accretes on a solid surface as a result of the surface phenomenon known as adsorption [11,12]. Adsorbents can frequently be reused after regeneration, and adsorption typically has excellent therapeutic efficacy.

Adsorption's ability is mostly dependent on the adsorbent's characteristics, hence creating an effective adsorbent is crucial for its widespread use in water treatment [13]. Polymers offer a wide range of applications due to their numerous recognition sites, high loading capacity, and simplicity of modification [14]. A good adsorbent should be resistant to acids, bases, reducing and oxidizing agents, be less soluble in water, and not be poisonous. The majority of dye adsorption processes are controlled by variables such as the starting concentration, dosage, interaction time, temperature, etc.

Chitosan is a biopolymer containing a linear polysaccharide based on glucosamine units that can be made by deacetylating chitin. Chitosan is regarded as a versatile and a non-toxic raw material, both biodegradable and frequently used [15]. It has been utilized in numerous industries, such as food production, agriculture, and medical, textiles, wastewater treatment, etc. However, its more widespread application was somewhat constrained due to its acidic Medium [16]. Chitosan that has been cross-linked is insoluble in acid solution, which increases its stability. However, cross-linking frequently comes at the expense of the hydroxyl and amino groups in chitosan, resulting in a reduction in chitosan's capacity for adsorption [17,18]. In this study A combination of $Nb_2O_5$, $Cr_2O_3$ and MnO2with chitosan is highly appealing when taking into account the disadvantages of chitosan and the good biological activities of the metal oxides listed above; yet, to our knowledge, data on this are still lacking. Here, innovative porous chitosan-metal oxide ($Nb_2O_5$, $Cr_2O_3$ and $MnO_2$) nanocomposites were easily made by forming the metal oxides in the chitosan matrix while they were still in place. An increase in positively charged traits would make anion dye removal easier [19-21].

- To prepare a protonated cross-linked chitosan is one of the study's goals.
- to examine the effects of various experimental conditions, including initial dye concentration, adsorbent dosage, and pH of dye solution.
- to look into the effects of this dye's pH on the adsorption process.

It is very water soluble. The CS/$Nb_2O_5$/$MnO_2$ and CS/$Nb_2O_5$/$Cr_2O_3$ ternary nanocomposite was characterized using a number of techniques, including X-ray diffraction (XRD), Fourier transform infrared spectroscopy (FTIR), and scanning electron microscopy (SEM). During the next experiments, which examined the effects of pH solution, starting dye concentration, adsorbent dose, and contact time, Utilizing the batch equilibrium method and UV-vis spectroscopy, it was discovered that this sample had a high adsorption capacity for dye removal. Additionally, the adsorption process's kinetics, isotherms, and thermodynamics have been identified. The information offers hope for

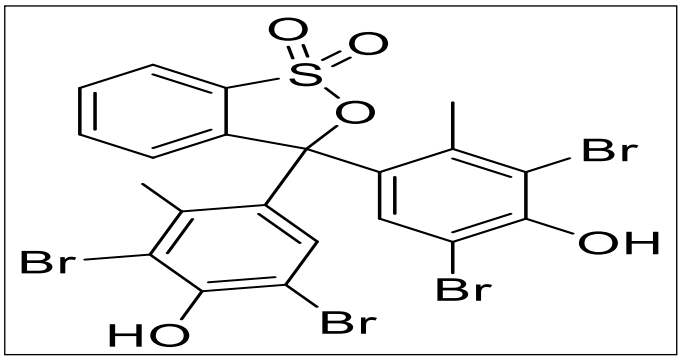


Fig. 1. Chemical structure of Bromocresol green (BCG).

several important inferences, such as economic viability and reusable adsorbent for color removal. We are consequently investigating the performance of a CS/$Nb_2O_5$/$MnO_2$ and CS/$Nb_2O_5$/$Cr_2O_3$ ternary nanocomposite (as an adsorbent) for the removal of Bromocresol green (BCG) from wastewater. The chemical name for bromocresol green

Fig. 1 is (2,6-dibromo-4-[7-(3,5-dibromo-4-hydroxy-2-meth y l - p henyl ) - 9 , 9 - d i o x o - 8 - o x a - 9 λ 6 - thiabicyclo[4.3.0]nona-1,3,5-trien-7-yl]-3-methyl-phenol)is a member of to the triphenylmethane family of dyes, which is employed in DNA agarose gel electrophoresis as a tracking dye and as a pH indicator [22].

## MATERIALS AND METHODS

### *Chemicals Used*

Water solutions were employed in this study. The ingredients, which included chitosan (99.5 percent), sodium hydroxide (99.8%)and acetone, were used exactly as they were purchased from Sigma-Aldrich (99.5 percent). The following chemicals were used without additional purification: Acetic acid (CH3CO2H (Sigma), niobium(v) oxide (Fluka, 99%), chromium(III) oxide, ethanol, and manganese (IV) oxide (Panreac, 98%).

### *Synthesis of CS/$Nb_2O_5$/$MnO_2$ and CS/$Nb_2O_5$/ $Cr_2O_3$ Adsorbent*

At first, 2 g chitosan was dissolved in 100 mL of distilled water/ 2 mL acetic acid under magnetic stirring for 1 hour at room temperature. Then, (1g $Nb_2O_5$ and 1g $MnO_2$) powder were added to a solution directly, the black mixture was dispersed in ultrasonic for 60 min. Afterward, 0.1 M of NaOH (pH=6) was added to the ultrasonic solution, and this mixture was reacted under magnetic stirrer for 4 h [23]. The resulting CS/$Nb_2O_5$/$MnO_2$ nanocomposite was washed with acetone, 100 ml of 1 M HCl, new distilled water, and a Buchner funnel. Finally, the product was dried for 24 hours at 90 °C in a vacuum oven. Similar to how CS/$Nb_2O_5$/$MnO_2$ nanowires were made, CS/$Nb_2O_5$/$Cr_2O_3$ nanowires were created using the same method.

### *Characterization of Adsorbent*

The CS/$Nb_2O_5$/$MnO_2$ and CS/$Nb_2O_5$/$Cr_2O_3$ were analyzed using FTIR, XRD, SEM, and UV-Vis. A PerkinElmer Spectrum One Fourier Transform Infrared spectrophotometer was used to obtain the spectra (FTIR). Before cataloging the scope of any influential polymer experiments. The Ministry of Science and Technology used an X-ray diffractor

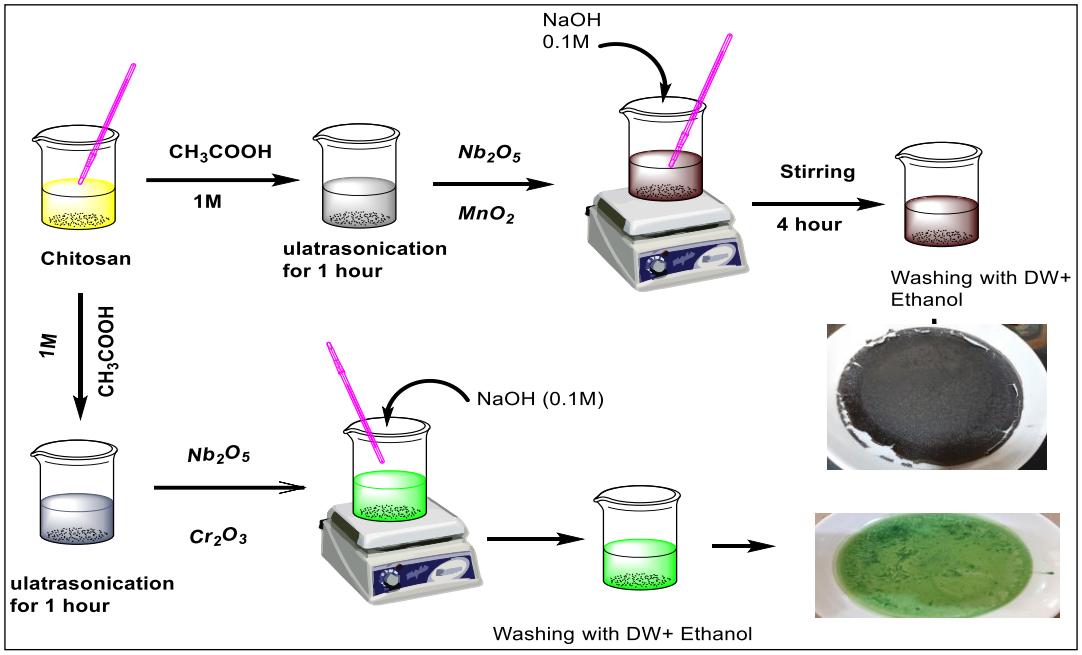


Fig. 2. Schematic of the synthesis of Chitosan/ $Nb_2O_5$, $Cr_2O_3$ and $MnO_2$ sample by in situ oxidative polymerisation with its proposed interactions.

(Model: Xrd-6000/shimadzu, Japan) operating at 40kV, 30 mA, and used a step size of 0.05°2 to scan between 5° and 80° 2 in order to examine the polymer composites' structural details. Thermo Fisher Scientific XL30 ESEM apparatus with a gas pedal voltage of 10 keV was used to examine the morphology of the outer layer of the polymer nanocomposites.

*Experiments on Batch Adsorption and experimental Design*

The as-synthesised CS/$Nb_2O_5$/$Cr_2O_3$ and CS/$Nb_2O_5$/$MnO_2$ nanocomposites are effective adsorbents for the filtration of water and wastewater due to their large surface area and strong adsorption capacities. Since methyl orange (BCG) is a organic pollution is a common industrial problem. effluent, this investigation determined its presence. A number of factors, including the pH of the solution, the amount of adsorbent used, the initial concentration of BCG dye, and the reaction time, were studied in relation to the removal of BCG dye and its adsorption onto CS/$Nb_2O_5$/$Cr_2O_3$ and CS/$Nb_2O_5$/$MnO_2$ nanocomposites. A

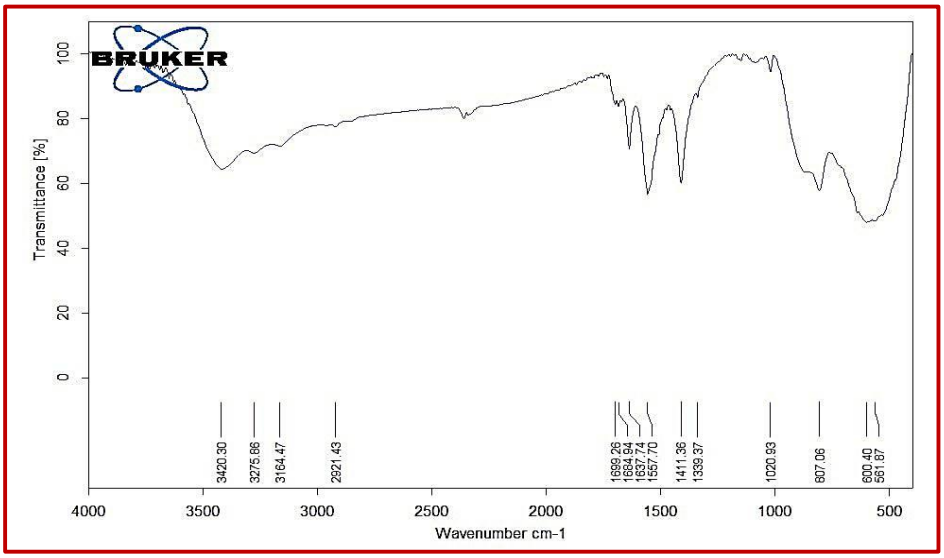


Fig. 3. FTIR spectra for CS /$Nb_2O_5$/$MnO_2$ sample.

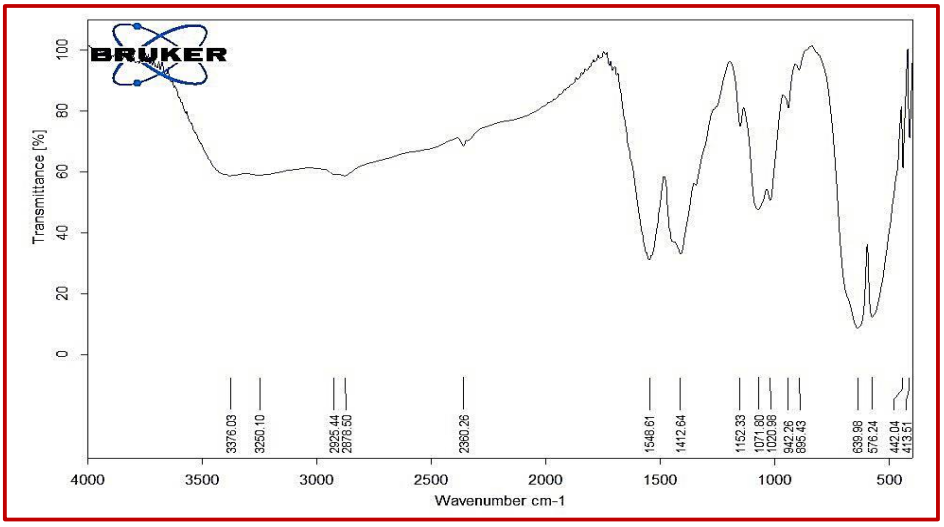


Fig. 4. FTIR spectra for CS/$Nb_2O_5$/$Cr_2O_3$ sample.

BCG dye adsorption equilibrium experiment was carried out using two 250 mL conical flasks with a constant adsorbent dosage (100 mg). with initial doses for 100 mL of BCG dye ranging from 5 to 50 mg/L. A pH meter was used to monitor the pH of the setups, which was adjusted to pH 7. (Oakton 550, USA). To ensure equilibrium conditions, the orbital shakers were shaken at a controlled speed of 300 rpm after 60 minutes. A UV-vis spectrophotometer (Cary 5000, USA) was used to measure the concentration of BCG before and after purification at its maximum wavelength of 615 nm. The percentage of dye removal (percent DR) was calculated using the following techniques: Eq. (1) as:

$$\text{Dye Removal} = \frac{(\text{ci} - \text{ce})}{\text{ci}} \times 100 \quad (1)$$

Where, Ci is the BCG dye's starting concentration (mg/L), and Ce is the dye's equilibrium concentration following adsorption (mg/L). The adsorption capacity (qe) was calculated using Eq. (2):

$$\text{qe} = \frac{(\text{ci} - \text{ce})\text{v}}{\text{m}} \quad (2)$$

Where, V is the volume of BCG dye solution (L), and M is the weight of the synthesized adsorbent (g) used.

## RESULTS AND DISCUSSION

### *Characterization of CS/$Nb_2O_5$/$Cr_2O_3$ and CS/$Nb_2O_5$/$MnO_2$*

#### *Fourier Transformation Infrared Spectrum (FTIR) Analysis*

For nanocomposites constructed of CS/$Nb_2O_5$/$Cr_2O_3$ and CS/$Nb_2O_5$/$MnO_2$, respectively, Figs. 3 and 4 show FTIR peaks in the 400–4000 cm-1 range. Figs. 1 and 2 show that all chitosan samples exhibit the peak at 1152,1020 cm-1, which results from the saccharide moiety [24-26], in addition to -CH stretching vibration at 2921 cm-1. While the discrete peaks at 1637 and 1557 cm-1 indicate -$NH_2$ bending vibration and 1399 cm-1 is related to stretching of amide, the strong band at 3420 cm-1 corresponds to -OH and -$NH_2$ stretching vibration. Wide peaks in the range of 1339–1412 cm-1 were caused by the M–O–M deformation vibration [27]. Additionally, M-OH and M-O bending vibration are responsible for the peaks in the 807-413 cm1 range. Characteristic peaks for the metal oxides as well as CS(chitosan) were present in the spectra of CS-$Nb_2O_5$/$MnO_2$ and CS-$Nb_2O_5$/$Cr_2O_3$.

#### *Xray Diffraction (XRD) Analysis*

The XRD examination can provide information on the creation of chitosan's semi-crystalline structure, crystalline chitosan-$Nb_2O_5$/$MnO_2$, and

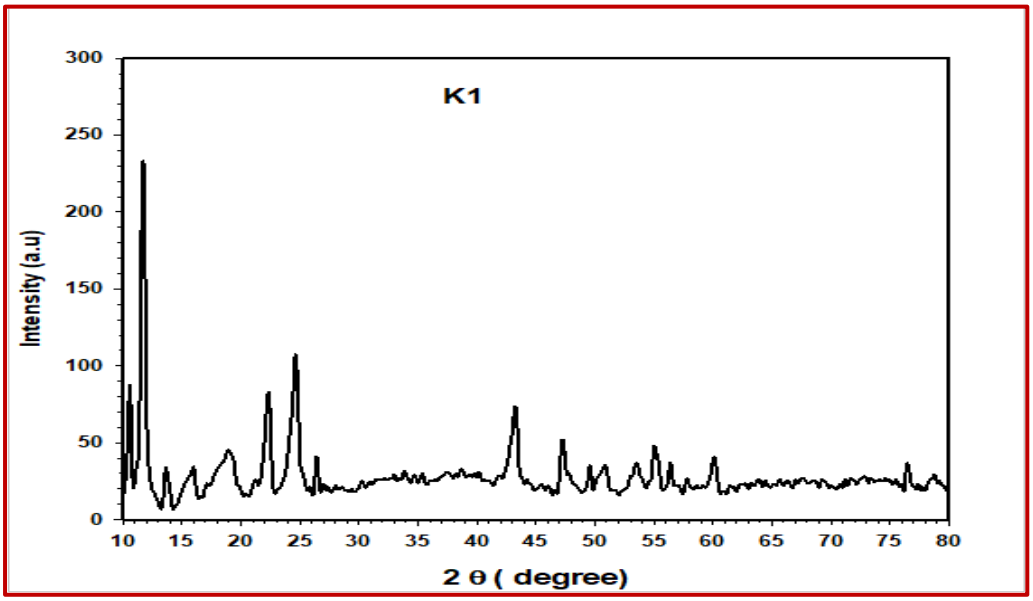


Fig. 5. XRD spectra for CS/$Nb_2O_5$/$MnO_2$ samples.

crystalline chitosan-$Nb_2O_5$/$Cr_2O_3$ structures (Fig. 5,6). the wide peaks were seen at 2θ = 11.7°, 22.2°, 24.5° ,43.2°,50.6°,60.55° and 76.65°. These pinnacles confrmed that formless construction was available CS/$Nb_2O_5$/$MnO_2$ in the lattice [28]. while The CS/$Nb_2O_5$/$Cr_2O_3$ nanocomposite XRD tops noticed were basically indistinguishable from the Chitosan precious stone planes 2θ = 11.78°, 22.4°, 24,4° 33.4°,36°,41.3°,50.05°,54.7°, 72.8° and 76.7°. separately, showing that there were adsorption associations between the metal oxides, some of a nanocrystalline structure ($Nb_2O_5$ and additionally $MnO_2$,$Cr_2O_3$) and chitosan network This suggests that the chitosan was collaborating with $Nb_2O_5$, $Cr_2O_3$ and $MnO_2$ in great precious stone construction. These outcomes (i.e., XRD), close by they have confirmed that the aniline monomer had been efficiently polymerized on the outer layer by FTIR measurements. of the $Nb_2O_5$, $Cr_2O_3$ and $MnO_2$ nanoparticles [29,30].

*Surface Characterization by SEM*

The distribution of metal oxides and the morphology of the nanocomposite Chitosan-$Nb_2O_5$/$MnO_2$ and chitosan-$Nb_2O_5$/$Cr_2O_3$ nanocomposite SEM images are shown in Figs. 7 and 8. SEM photos show the instrument characteristics, accelerating voltage, spot size, magnification, and working distance. The concentration of salt, the amount of chitosan in the solution, the temperature, and the solution's pH all

have an impact on the shape and particle size of $Nb_2O_5$, $MnO_2$ and $Cr_2O_3$ [31]. The SEM pictures show the presence of some sort of agglomeration-type structure. The clearly apparent black and white patches on the nanocomposite surface. Chitosan-$Nb_2O_5$/$MnO_2$ nanocomposite's SEM-EDX examination revealed the existence of C,O,N,Nb,Mn at concentrations of 15.46%, 47.52%, 2.83%, 27.53%, and 6.66% , respectively. Chitosan-$Nb_2O_5$/$Cr_2O_3$ nanocomposite's EDX spectra revealed the presence of C,O,N,Nb,Cr at percentages of 5.14%, 50.43%, 3.93%, 9.19%, and 31.31%, respectively.

*Zeta Potential Analysis*

The electric potential formed by the presence of a charge on the particle surface, which can be positive or negative in polarity depending on the chemistry of the particles, is known as zeta potential. The degree of repulsion between similarly charged particles in a formulation is measured by the zeta potential**.** Particle aggregation during storage is prevented by repulsive forces. As a result, a formulation's zeta potential indicates its likely physical stability. Figs. 9 and 10 shows the changes in the zeta potential. In addition, particle size. The pH was 7.3, the value of the zeta potential value was 19.38 mV , and it does seem to depend on the pH value. The zeta potential increases with decreasing value of

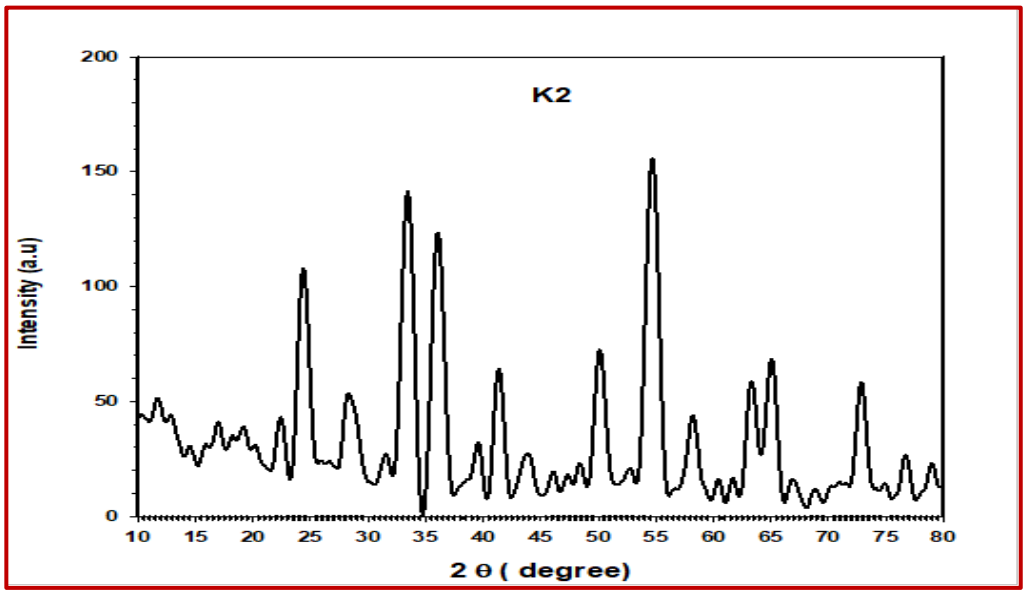


Fig. 6. XRD spectra for CS/$Nb_2O_5$/$Cr_2O_3$ samples.

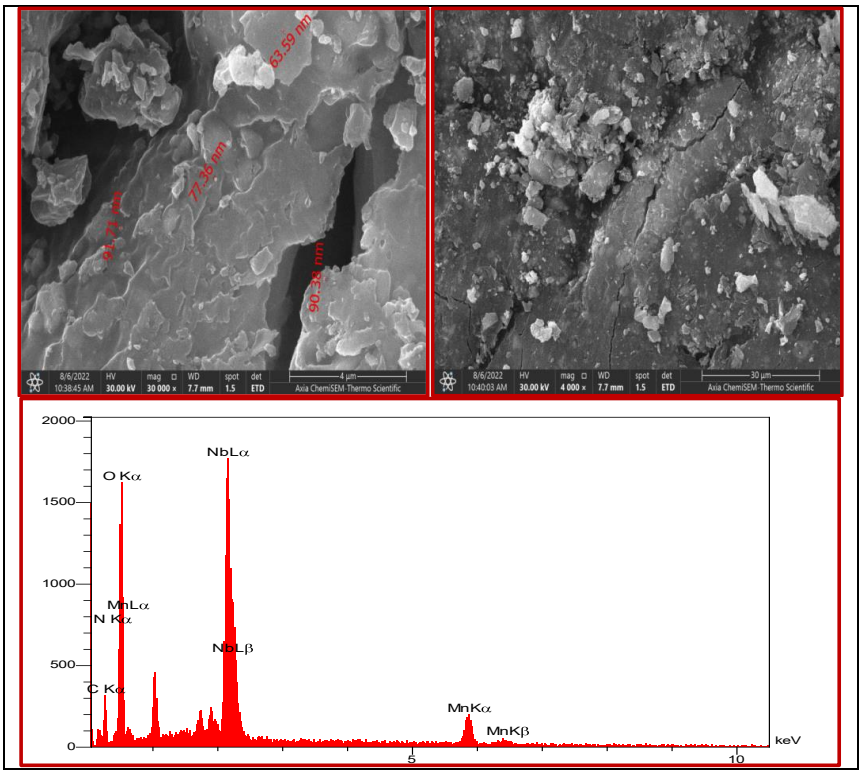


Fig. 7. SEM and EDX micrographs of CSI/$Nb_2O_5$/$MnO_2$ nanocomposite.

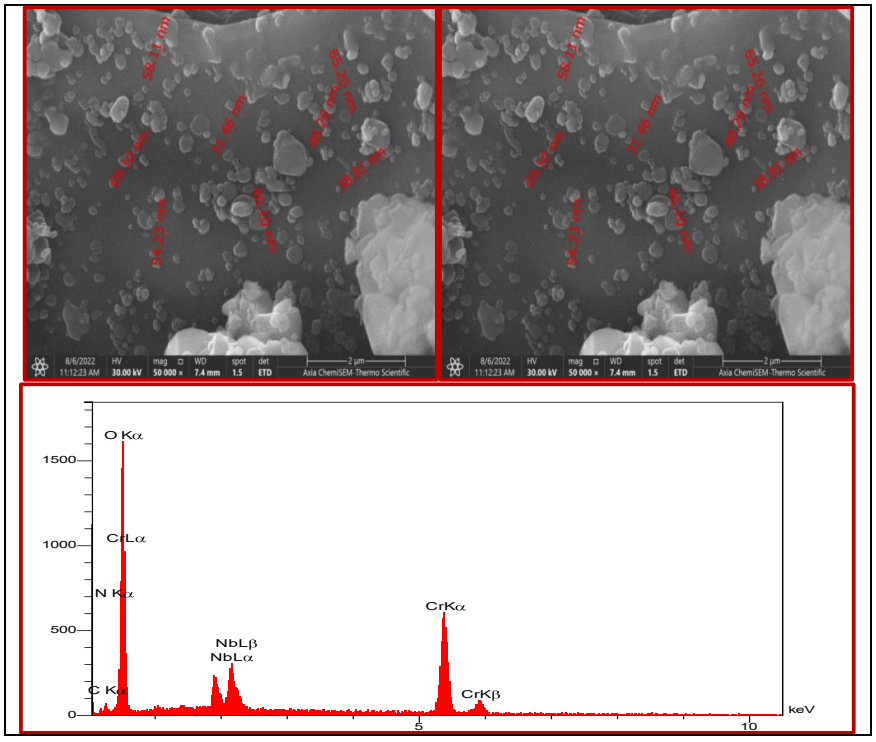


Fig. 8. SEM and EDX micrographs of CS/$Nb_2O_5$/$Cr_2O_3$ nanocomposite.

pH. The dependence of the zeta potential of the dispersion of CS/$Nb_2O_5$/$Cr_2O_3$ on the pH value as in Fig. 9 is similar to all the applied synthesis methods. The zeta potential is positive for pH values less than 5.5 and negative when the pH increases with the isoelectric point around pH =

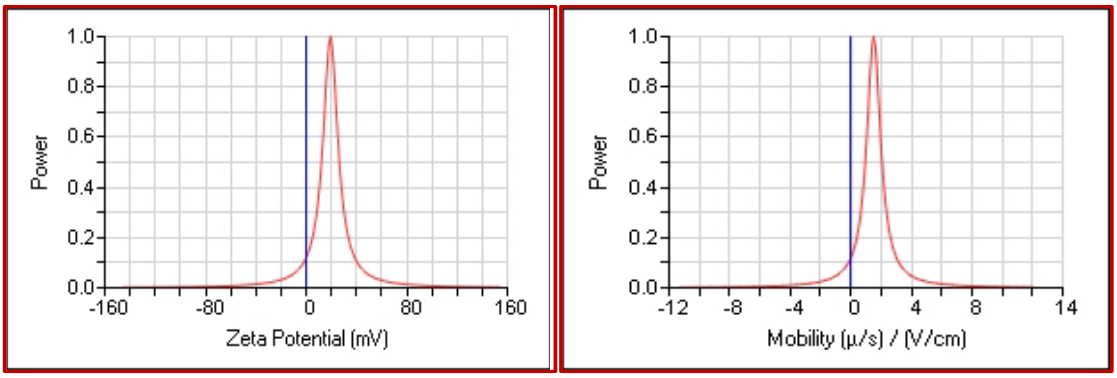


Fig. 9. Zeta potential curves for CS/$Nb_2O_5$/$Cr_2O_3$.

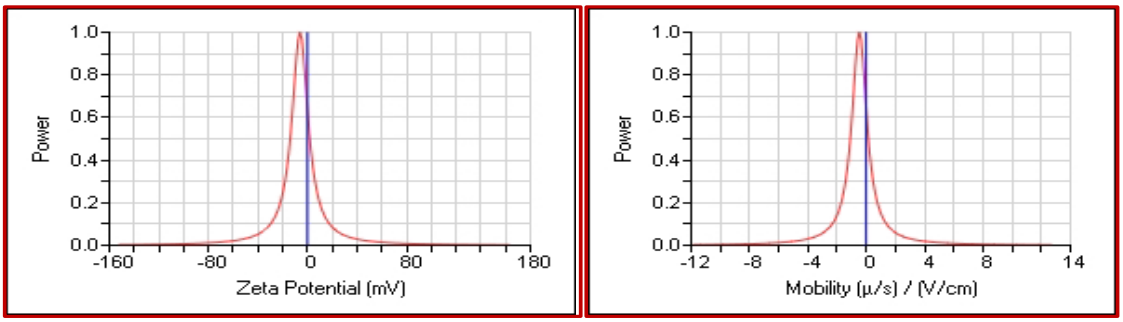


Fig. 10. Zeta potential curves for CS/$Nb_2O_5$/$MnO_2$.

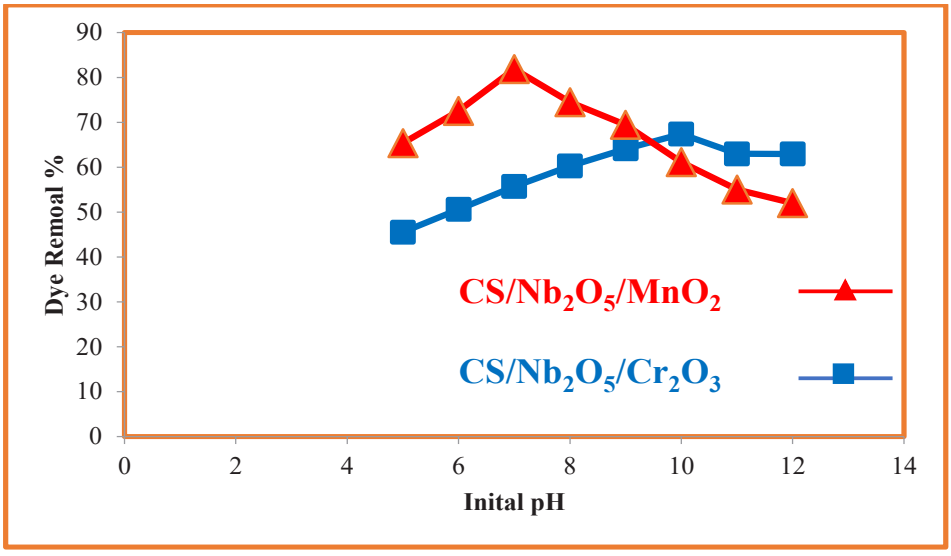


Fig. 11. Effect of pH on removal of BCG Dye.

5.6. The zeta-potential depends on the interaction between water ions and the nanoparticles.

This is due to negatively charged molecules on surfaces repelling negatively charged nanoparticles. However, other researchers believe that there are just a few cationic spots on cell surfaces that can adsorb and bind to negatively charged particles. They theorized that when negatively charged NPs connect to cationic sites, they form clusters (agglomerates) due to the repulsion shown by the vast negatively charged domains of the cell surface. Furthermore, the charge density on the cell surface is reduced by the bound NPs, which may facilitate the adsorption of other free NP.

*Absorption Behavior of BCG CS/$Nb_2O_5$/$Cr_2O_3$ and CS/$Nb_2O_5$/$MnO_2$ Adsorbent Nanocomposites*

*Effect of pH on BCG dye Removal*

The adsorbent's nature, surface characteristics, and ionization/dissociation of the adsorbate molecule are all significantly influenced by the

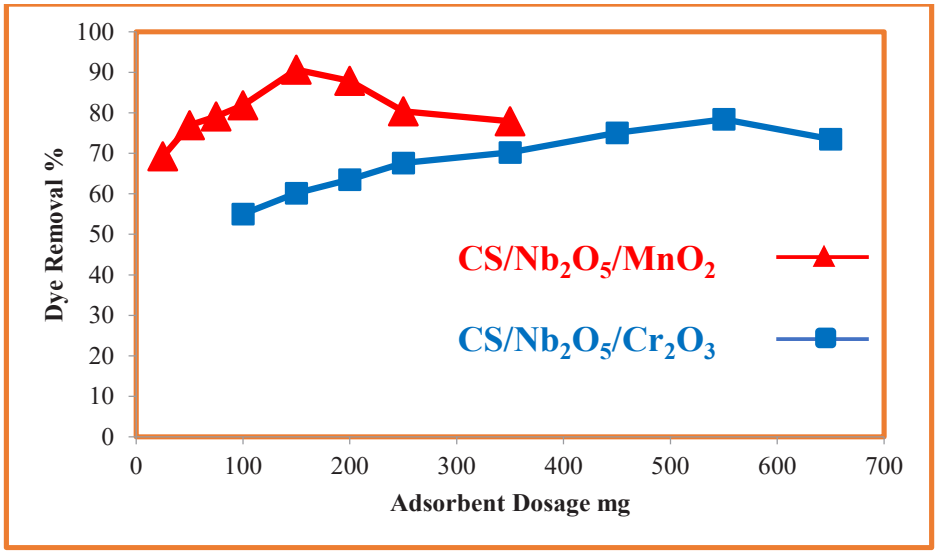


Fig. 12. Effect of adsorbent dosage on the removal of BCG dye.

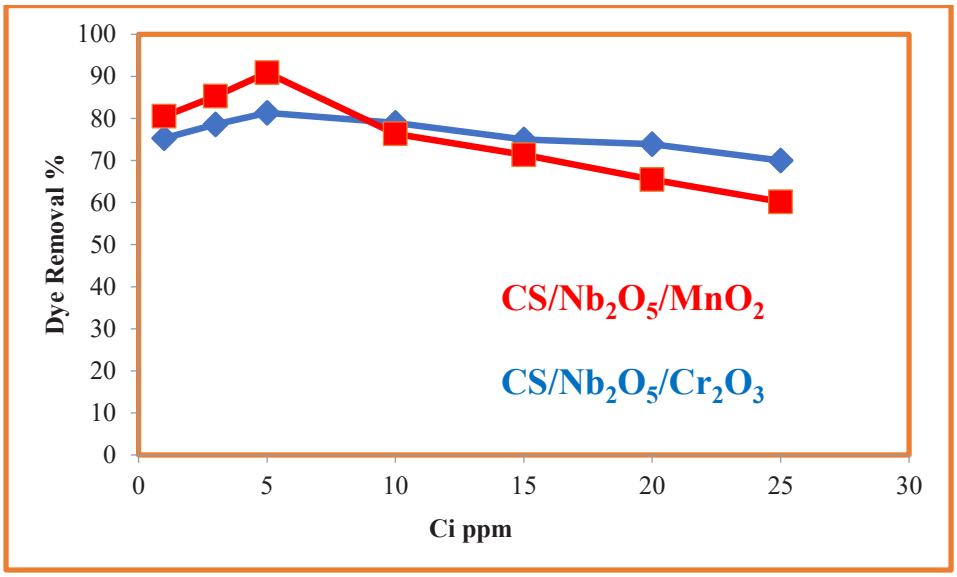


Fig. 13. Effect of initial concentration of MO dye on removal process.

pH of the sample. In the pH range of 5–12.0, the impact of sample pH on the adsorption of BCG by nanocomposite materials made of CS/$Nb_2$O5/$Cr_2O_3$ and CS/$Nb_2O_5$/$MnO_2$. It is possible to explain the greater dye removal at acidic pH in terms of the electrostatic interaction between the dye and the chitosan [32] 0.1 M HCl or 0.1 M NaOH were used to regulate the pH during an experiment, and a pH meter was used to record the results. The initial BCG dye concentration was kept constant at 5 mg/L, 300 rpm, 100 mg, and 298 K for CS/$Nb_2O_5$/$MnO_2$ and while the CS/$Nb_2$O5/$Cr_2O_3$ initial concentration at 10 mg/L, 300 rpm, 250mg, and 298 K Fig. 11 shows that the adsorption efficiency steadily increased and peaked at pH 7 for CS/$Nb_2O_5$/$MnO_2$ (about 81.86 percent) and pH 10 for CS/$Nb_2O_5$/$Cr_2O_3$(about 67.4 percent) respectively. When the alkaline pH exceeded 12, it then started to decline. The amino group on the surface of chitosan attracted the hydroxonium ion on the

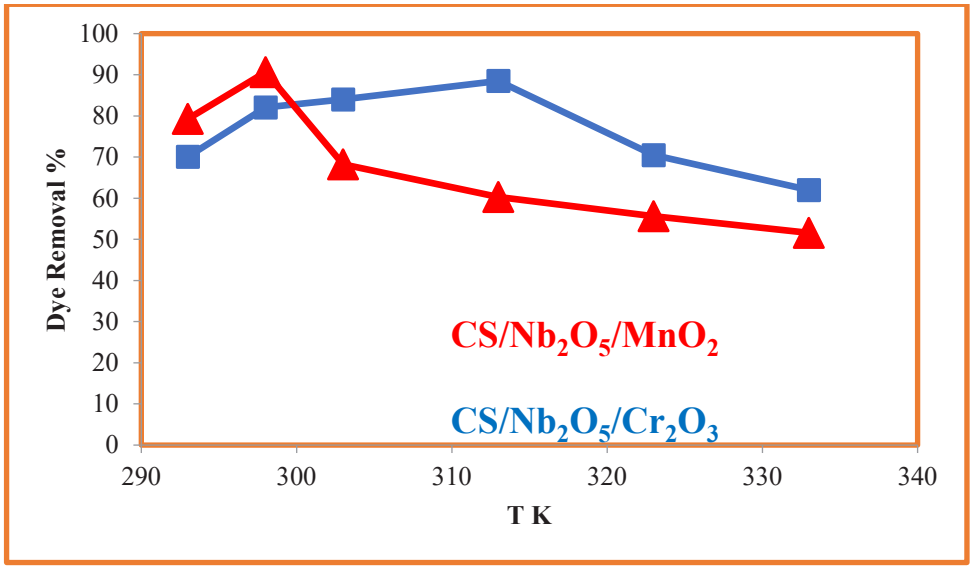


Fig. 14. Effect of Temperature of BCG dye on removal process.

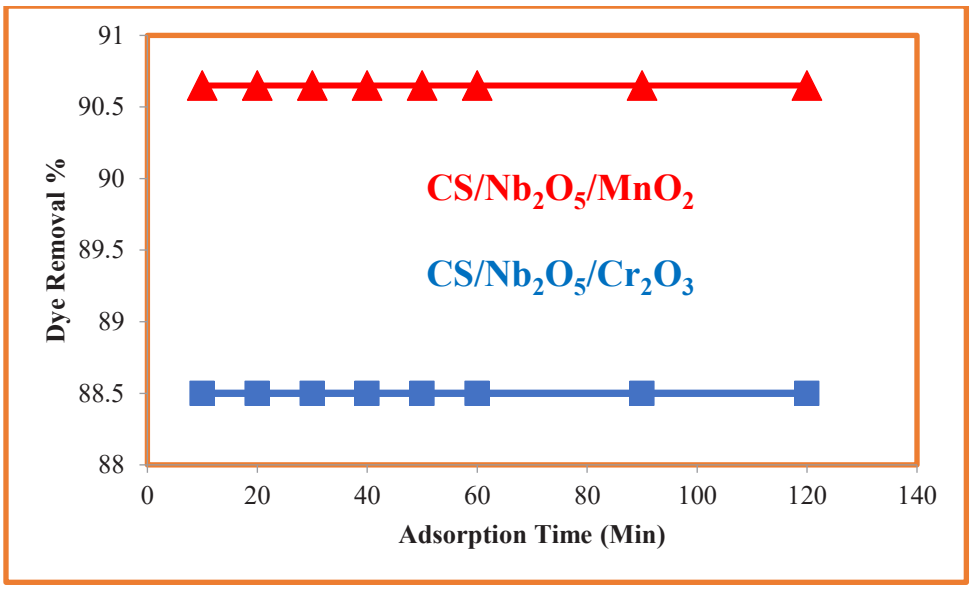


Fig. 15. Effect of Adsorption time on removal of BCG dye.

surface of the solution, increasing the adsorption capacity found at lower pH [33]. Additionally, debutination took place at the active areas of the adsorbent surface at baseline pH levels above 7, leading to OH repulsion on the surface [39,40]. Lower adsorption capacity was caused by competition for adsorption sites between the dye and excess H+ and OH in the acidic or basic solution.

*Effect of Adsorbent Dosage*

To determine the effects of adsorbent dosage on BCG dye clearance, removal experiments were carried out using various doses of CS/$Nb_2O_5$/$Cr_2O_3$ and CS/$Nb_2O_5$/$MnO_2$, ranging from 25 to 650 mg. Fig. 12 displays for each the effect of adsorbent dosage on removal efficacy. It was shown that increasing the adsorbent dosage from 100 to 550 mg for CS/$Nb_2O_5$/$Cr_2O_3$ and from 25 to 150 mg for CS/$Nb_2O_5$/$MnO_2$ considerably increased the removal effectiveness of the BCG dye from 67.4 to 78.4% and 81.86 to 90.65 percent, respectively. This may be because more active sites became available when the adsorbent dosage was raised, and eventually, at a dosage of 550, 150mg, the associated equilibrium was established. In light of this, an adsorbent dosage of 550,150 mg for CS/$Nb_2O_5$/$Cr_2O_3$ and CS/$Nb_2O_5$/$MnO_2$ respectively were chosen for other experiments.

*Effect of Differences in the Process of Removing BCG dye's Initial Concentration*

As shown in Fig. 13, the initial dye concentration has a considerable impact on the

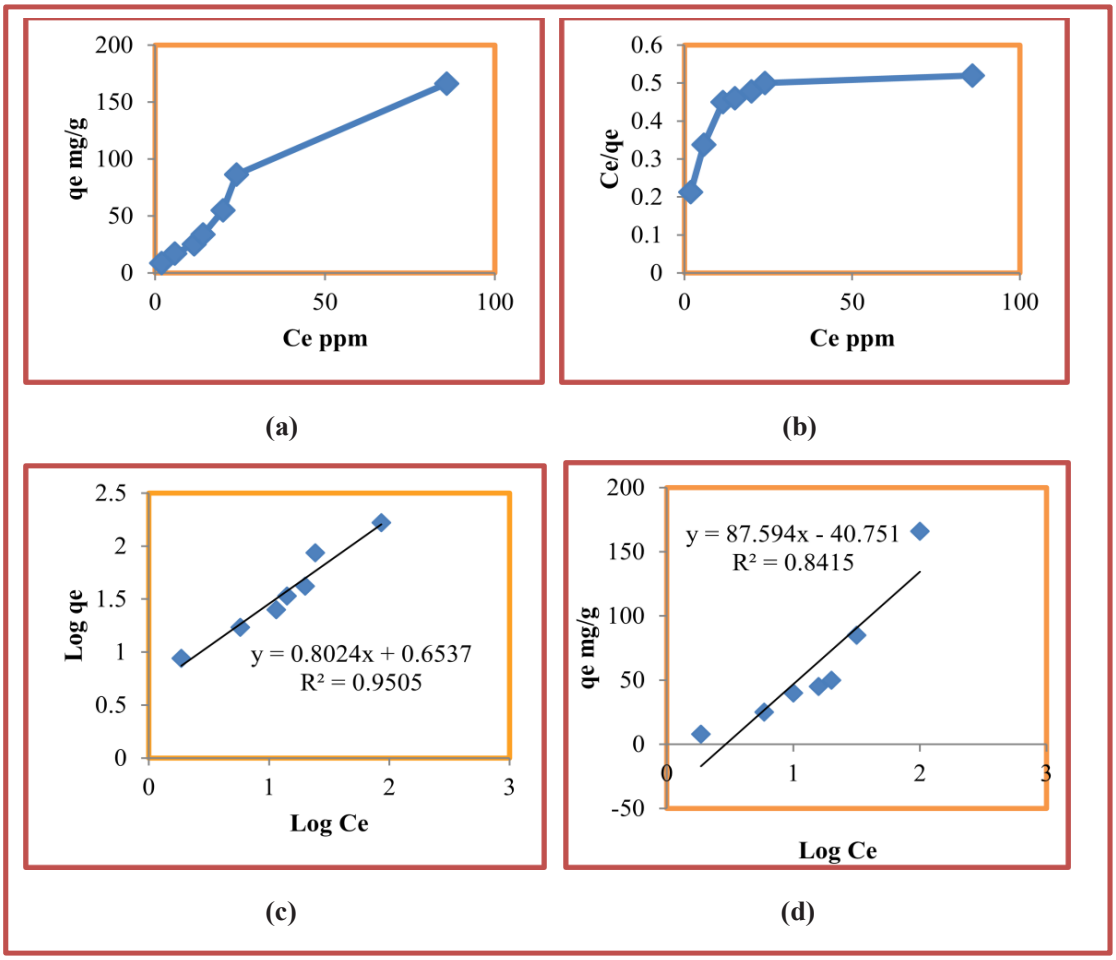


Fig. 16. a Adsorption isotherms of BCG onto CS/$Nb_2O_5$/ $Cr_2O_3$ adsorbents (conditions: pH 10; dosage=550 mg; V=100 mL; time=10 min; T=313 K); fitting the adsorption isotherm curves of BCG dye of adsorbents: b Langmuir isotherm model, c Freundlich isotherm model; d Temkin isotherm model.

adsorption potentials of the adsorbents. The BCG concentrations for this experiment ranged from (1 to 25) mg/L for both the CS/$Nb_2O_5$/$Cr_2O_3$ and CS/$Nb_2O_5$/$MnO_2$ systems, while the adsorbent dose, time interval, pH, and temperature were maintained at( 550,150 g, 30 min, pH=10,7, and T=298K) respectively. Due to a paucity of surface sites required for the concentration of the dye, the percentage of BCG that is adsorbed decreases as BCG concentration rises. Additionally, it can be linked to the fact that the accessible solutes are absorbed more quickly when the BCG concentration is lower [34]. Additionally, the high percentage of MO dye removal by CS/$Nb_2O_5$/$Cr_2O_3$ and CS/$Nb_2O_5$/$MnO_2$ nanocomposite materials may be explained by their stronger electrostatic interactions as well as their higher surface areas. The modified CS/$Nb_2O_5$/$Cr_2O_3$ and CS/$Nb_2O_5$/$MnO_2$ nanocomposite's porosity.

*Effect of Temperature on Removal of BCG Dye*

The impact of temperature on adsorption is one of the most crucial factors used to establish the nature of the adsorption process. Fig. 14 illustrates the relationship between temperature and BCG adsorption, which was studied at a temperature range of 293-333K with fixed other conduction (550 mg, 5 mg/L, and pH 10 for 30 min for CS/$Nb_2O_5$/$Cr_2O_3$, and (150 mg, 5 mg/L, and pH 7 for 30 min for CS/$Nb_2O_5$/$MnO_2$, respectively). For CS/$Nb_2O_5$/$Cr_2O_3$, bromocresol green dye was rapidly adsorbed from 298 to 323 K, whereas sluggish adsorption from 323 to 333 K produced the highest clearance percentages (88.5% at 313 K). although the ideal conditions for both adsorption and dye removal are at 298 K

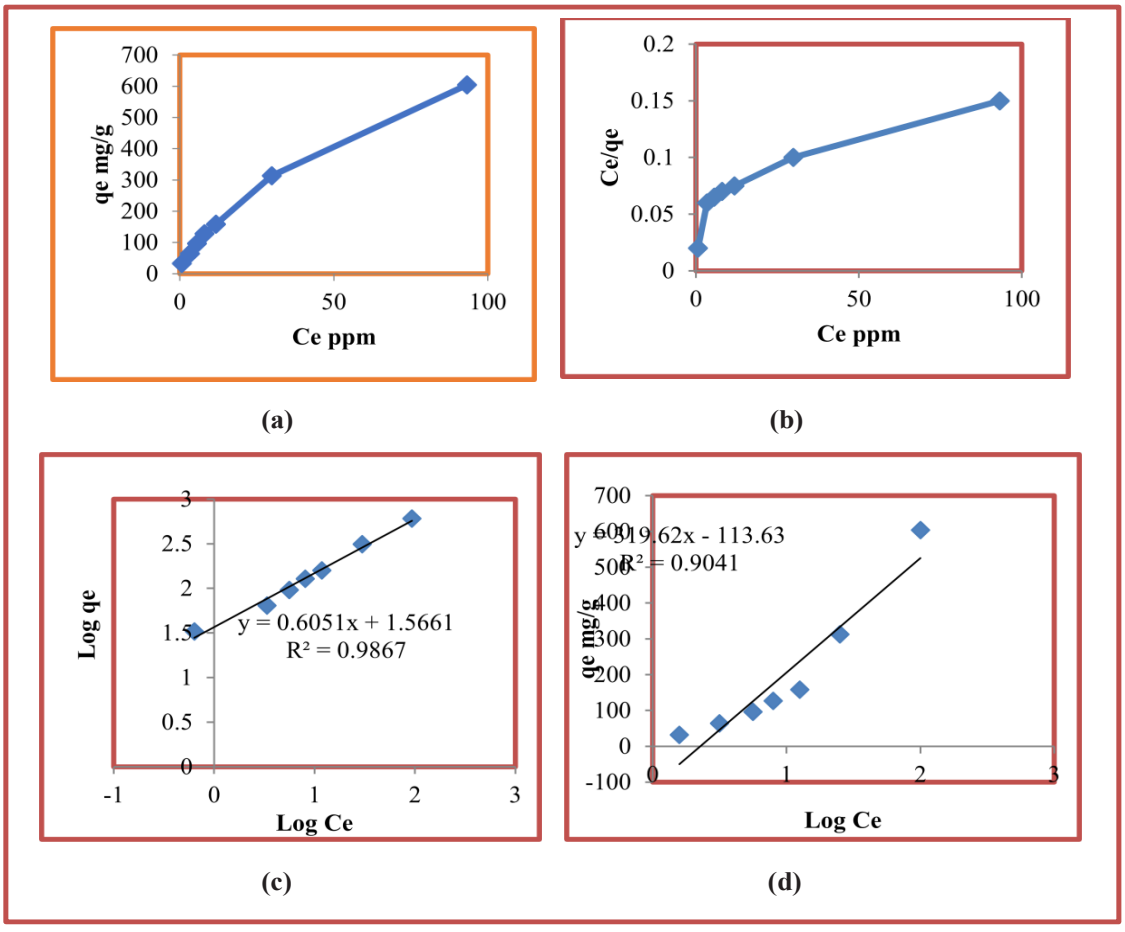


Fig. 17. a. Adsorption isotherms of BCG onto CS/$Nb_2O_5$/ $MnO_2$ adsorbents (conditions: PH 7; dosage=150 mg; V=100 mL; time=10 min; T=298 K); fitting the adsorption isotherm curves of BCG dye of adsorbents: b Langmuir isotherm model, c Freundlich isotherm model; d Temkin isotherm model.

(removal percentage 90.65% for CS/$Nb_2O_5$/$MnO_2$ [35]. The capacity of the adsorbent to adsorb a particular molecule in equilibrium can fluctuate depending on temperature. The adsorption of the dye reduces with rising temperature, indicating an exothermic adsorption process, whereas a fall in temperature indicates an endothermic adsorption reaction. In addition to the low temperature of the species that are adsorbed and the limited number of active sites, the physical connection between both organic compounds, including dyes and the active sites of adsorption, reduced with rising temperature [36,37].

*Effect of Adsorption Time*

Another important the adsorption time is a factor in the color removal process. The effects of adsorption time on the adsorption of BCG dye onto various surfaces were examined in a series of experiments with adsorption times between 10 and 120 minutes. the CS/$Nb_2O_5$/$Cr_2O_3$ and CS/$Nb_2O_5$/$MnO_2$ adsorbents were investigated. The outcomes are displayed in Fig. 15. At the beginning of the adsorption phase, a sharp increase in the percentage adsorbed was seen. This is because there were a lot of positively charged surfaces on the adsorbent at first, which enhanced the concentration gradient and the adsorption process' driving force. After 10 minutes, equilibrium concentration was reached. that the rate of BCG dye removal was extremely rapid during the first 10 min, during which time approximately 88.5% percent of the BCG dye molecules were adsorbed by the CS/$Nb_2O_5$/$Cr_2O_3$ and 90.65% percent by the CS/$Nb_2O_5$/$MnO_2$ adsorbents. Due to the existence of additional adsorption sites and a high solution concentration, the anions in BCG quickly interacted with the chitosan during the initial contact period, resulting in this high rate of adsorption [38].

*Batch BCG Dye Adsorption Studies*

Experimentally, it was found that the CS/$Nb_2O_5$/$Cr_2O_3$ and CS/$Nb_2O_5$/$MnO_2$ adsorbents' adsorption capabilities were best at pH 10 and pH 7, respectively, when used with 100 mL solutions of BCG dye with concentrations ranging from 5 to 100 mg/L at room temperature (298 K) (Fig. 16a). The maximal adsorption capabilities of the CS/$Nb_2O_5$/$Cr_2O_3$ and CS/$Nb_2O_5$/$MnO_2$ adsorbents were equal to 166 mg/g and 604 mg/g, respectively, as can be seen from this figure. Three fundamental isotherm models, specifically the Langmuir, Freundlich, and Temkin models), were used to fit the adsorption data in order to assess the mechanism of adsorption and provide information on the maximum adsorption capacity (qm) for the relevant adsorbent [39,40]. Fig. 16 displays the graphs for the linearized equation isotherm parameters for BCG dye elimination at 298 K. Table 1 lists the three equations for the isotherm models for adsorption at room temperature along with their maximum adsorption capacities (qm), correlation coefcients (R2), and other information. The Langmuir model had a number of presumptions, including that the adsorbate would bind to the adsorbent in a monolayer on a uniform surface [41]. The Langmuir equation is given in Eq. (3) .

$$\frac{Ce}{qe} = \frac{Ce}{qm} + \frac{t}{qmKL} \quad (3)$$

Where, qm and qe stand for the BCG dye's maximum (mg/g) and empirical (qe) adsorption capacities, respectively. After the adsorption process, Ce is the amount of BCG dye that is still present in the solution and KL is the Langmuir constant (L/ mg). In order to determine the adsorption capacity, Ce/qe versus Ce was plotted.

Table 1. Adsorption Langmuir, Freundlich, and Temkin model isotherm parameters for BCG dye by CS/$Nb_2O_5$/$Cr_2O_3$ and CS/$Nb_2O_5$/$MnO_2$ .

| Isotherms | Parameters | CS/$Nb_2O_5$/$Cr_2O_3$ | CS/$Nb_2O_5$/$MnO_2$ |
|---|---|---|---|
| Langmuir | $Q_m$ | 434.78 | 909 |
| | $K_L$ | 0.01 | 0.021 |
| | $R^2$ | 0.46 | 0.84 |
| Freundlich | $K_F$ | 4.5 | 36.82 |
| | n | 1.25 | 1.66 |
| | $R^2$ | 0.95 | 0.9867 |
| Temkin | A | 87.5 | 319.6 |
| | B | 40.7 | 113.6 |
| | $R^2$ | 0.85 | 0.9041 |

(Fig. 16b).

where the gradient and intercept of this (straight) line were used to estimate qm and KL, respectively. The Freundlich model is used to fit multilayer adsorption onto a heterogeneous surface, and the postulated adsorption process is physisorption, which happens as a result of van der Waals interactions. Eq provides the Freundlich equation (4).

$$\log qe = \log KF + \frac{1}{n} \log ce \quad (4)$$

According to Eq. (4), KF stands for the Freundlich constant, adsorption capacity (mg/g), and heterogeneity factor (n), which stands for the bond distribution. By graphing log qe against log Ce, the Freundlich linear equation was discovered. KF and n were then mathematically calculated from the intercept and gradient, respectively, of this linear connection (Fig. 16c). Eq. (5) specifies the Temkin equation, and the Temkin isotherm model makes significant assumptions about heterogeneous surface energy and non-uniform distribution of sorption heat on adsorbents[42].

$$qe = A + B \log Ce \quad (5)$$

Where, A is the Temkin isotherm constant (L/g) and B is a constant related to the heat of sorption (J/mol). Plots of qe against log Ce were used to arrive at the Temkin linear equation (Fig. 16d). The gradient and intercept of the straight line, respectively, provide the values of B and A. The parameters calculated for the Langmuir, Freundlich, and Temkin models are listed in Table 1The Langmuir isotherm appears to best describe the adsorption of BCG dye onto PANI/$Nb_2O_5$/$Cr_2O_3$ and CS/$Nb_2O_5$/$MnO_2$ adsorbents, as evidenced by the coefcients of determination (R2) for the fts of the experimental data to the three isotherms, which showed greater R2 (0.95 and 0.9867) and experimental equilibrium capacities (qe) This implies that both the CS/$Nb_2O_5$/$Cr_2O_3$ and CS/$Nb_2O_5$/$MnO_2$ adsorbents have strong BCG dye adsorption sites, and that the adsorption mechanism is monolayer in nature.

*Recyclability Study*

The CS/$Nb_2O_5$/$MnO_2$ and CS/$Nb_2O_5$/$Cr_2O_3$ nanocomposite's excellent recyclability suggests that the method may actually be useful for water purification. Under the ideal conditions described below, the recyclability was tested for 4 consecutive BCG dye adsorption-desorption cycles. For CS/$Nb_2O_5$/$Cr_2O_3$: pH 10; dosage: 550 mg; volume: 100 mL; time: 10 min; temperature: 313 K; and for CS/$Nb_2O_5$/$MnO_2$: PH 7; dosage: 150 mg; volume: 100 mL; time: 10 min; temperature:

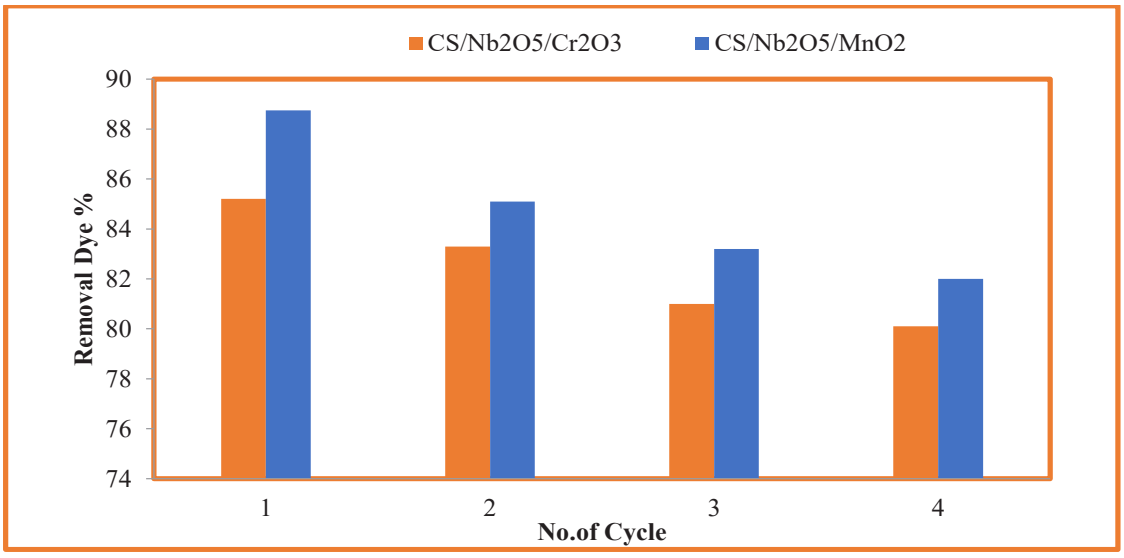


Fig. 18. Number of adsorption–desorption cycles using MO dye for CS/$Nb_2O_3$/$MnO_2$ and CS/$Nb_2O_5$/$Cr_2O_3$ (conditions: pH 7,10; doses = 150,550 mg; *Ci* = 5 mg/L; *V* = 100 mL; time = 10 min; *T* = 298,313 K).

298 K. The consumed quantity was magnetized out of the aqueous solution, rinsed with ethanol and deionized water, dried at 75 °C for four hours, and then put back into use for the following cycle of BCG dye adsorption. After then, it was discovered that the adsorption efficiency for the CS/$Nb_2O_5$/$MnO_2$ and CS/$Nb_2O_5$/$Cr_2O_3$ mixtures had both decreased from 90.65% to 82% and from 88.55% to 80.1%, respectively.(Fig. 18).

## CONCLUSION

In current study, two types of the nanocomposite CS/$Nb_2O_3$/$MnO_2$ and CS/$Nb_2O_5$/$Cr_2O_3$ as a new adsorbent were first prepared and characterised then used to remove of methyl orange dye. The physical and chemical of the nanocomposites such as structural, morphological, particle size and functional groups of the fabricated CS/$Nb_2O_3$/$MnO_2$ and CS/$Nb_2O_5$/$Cr_2O_3$were established via XRD, FE-SEM, FTIR, UV–Vis, and Zeta potential. The results have shown that the CS/$Nb_2O_3$/$MnO_2$ material sample has a higher adsorption capacity than CS/$Nb_2O_5$/$Cr_2O_3$ in terms of BCG removal, The maximal adsorption capabilities of the adsorbents were equal to 604 mg/g and 166 mg/g, respectively. The optimum conditions for the bromocresol green reactions with Chitosan /$Nb_2O_5$/$MnO_2$ where the dose was 150 mg, temperature 298 K, and pH value was 7, while with Chitosan /$Nb_2O_5$/$Cr_2O_3$ Nanocomposites the dose was 550 mg, temperature 313, and pH value was 10.

## CONFLICT OF INTEREST

The authors declare that there is no conflict of interests regarding the publication of this manuscript.

## REFERENCES


1. Vandenbossche M, Jimenez M, Casetta M, Traisnel M. Remediation of Heavy Metals by Biomolecules: A Review. Crit Rev Environ Sci Technol. 2014;45(15):1644-1704.
2. Khan M, Lo IMC. A holistic review of hydrogel applications in the adsorptive removal of aqueous pollutants: Recent progress, challenges, and perspectives. Water Res. 2016;106:259-271.
3. Katheresan V, Kansedo J, Lau SY. Efficiency of various recent wastewater dye removal methods: A review. Journal of Environmental Chemical Engineering. 2018;6(4):4676-4697.
4. Kos L. Effectt of Using Coagulants on Sedimentation Sludge Properties and Quality of Textile Wastewater. Fibres and Textiles in Eastern Europe. 2017;25(0):126-120.
5. Crini G, Lichtfouse E. Advantages and disadvantages of techniques used for wastewater treatment. Environ Chem Lett. 2018;17(1):145-155.
6. Aguilar-Ascón E, Marrufo-Saldaña L, Neyra-Ascón W. Reduction of Total Chromium Levels from Raw Tannery Wastewater via Electrocoagulation using Response Surface Methodology. Journal of Ecological Engineering. 2019;20(11):217-224.
7. Fu W, Chen H, Yang S, Huang W, Huang Z. Poly(diallyldimethylammonium-$MoS_4$) based amorphous molybdenum sulphide composite for selectively mercury uptake from wastewater across a large pH region. Chemosphere. 2019;232:9-17.
8. Wu M, Hu Y, Liu R, Lin S, Sun W, Lu H. Electrocoagulation method for treatment and reuse of sulphide mineral processing wastewater: Characterization and kinetics. Science of The Total Environment. 2019;696:134063.
9. Siekmeier R, Hofmann T, Scheuch G, Pokorski M. Aerosolized GLP-1 for Treatment of Diabetes Mellitus and Irritable Bowel Syndrome. Advances in Experimental Medicine and Biology: Springer International Publishing; 2014. p. 23-38.
10. Al-Musawi TJ, Mengelizadeh N, Al Rawi O, Balarak D. Capacity and Modeling of Acid Blue 113 Dye Adsorption onto Chitosan Magnetized by $Fe_2O_3$ Nanoparticles. Journal of Polymers and the Environment. 2021;30(1):344-359.
11. Hethnawi A, Nassar NN, Manasrah AD, Vitale G. Polyethylenimine-functionalized pyroxene nanoparticles embedded on Diatomite for adsorptive removal of dye from textile wastewater in a fixed-bed column. Chem Eng J. 2017;320:389-404.
12. Zhou Y, Hu Y, Huang W, Cheng G, Cui C, Lu J. A novel amphoteric β-cyclodextrin-based adsorbent for simultaneous removal of cationic/anionic dyes and bisphenol A. Chem Eng J. 2018;341:47-57.
13. Nakhjiri MT, Bagheri Marandi G, Kurdtabar M. Adsorption of Methylene Blue, Brilliant Green and Rhodamine B from Aqueous Solution Using Collagen-g-p(AA-co-NVP)/$Fe_3O_4$@$SiO_2$ Nanocomposite Hydrogel. Journal of Polymers and the Environment. 2019;27(3):581-599.
14. Bayramoglu G, Akbulut A, Liman G, Arica MY. Removal of metal complexed azo dyes from aqueous solution using tris(2-aminoethyl)amine ligand modified magnetic p(GMA-EGDMA) cationic resin: Adsorption, isotherm and kinetic studies. Chem Eng Res Des. 2017;124:85-97.
15. Gao Y, Wang X, Zhang Y, Li J, Zhang H, Li J. Novel fabrication of bi-metal oxide hybrid nanocomposites for synergetic enhancement of in vivo healing and wound care after caesarean section surgery. Int Wound J. 2022;19(7):1705-1716.
16. Yu J, Wang D, Geetha N, Khawar KM, Jogaiah S, Mujtaba M. Current trends and challenges in the synthesis and applications of chitosan-based nanocomposites for plants: A review. Carbohydr Polym. 2021;261:117904.
17. Razmi FA, Ngadi N, Wong S, Inuwa IM, Opotu LA. Kinetics, thermodynamics, isotherm and regeneration analysis of chitosan modified pandan adsorbent. Journal of Cleaner Production. 2019;231:98-109.
18. Ren L, Xu J, Zhang Y, Zhou J, Chen D, Chang Z. Preparation and characterization of porous chitosan microspheres and adsorption performance for hexavalent chromium. Int J Biol Macromol. 2019;135:898-906.
19. Tavizón-Pozos JA, Chavez-Esquivel G, Suárez-Toriello VA, Santolalla-Vargas CE, Luévano-Rivas OA, Valdés-Martínez OU, et al. State of Art of Alkaline Earth Metal Oxides Catalysts Used in the Transesterification of Oils for Biodiesel

Production. Energies. 2021;14(4):1031.
20. El Nahrawy AM, Mansour AM, Abou Hammad AB, Ibrahim RS, Abouelnaga AM, Abdel-Aziz MS. Optical, Functional Impact and Antimicrobial of Chitosan/Phosphosilicate/$Al_2O_3$ Nanosheets. Journal of Inorganic and Organometallic Polymers and Materials. 2020;30(8):3084-3094.
21. Youssef AM, El-Nahrawy AM, Abou Hammad AB. Sol-gel synthesis and characterizations of hybrid chitosan-PEG/calcium silicate nanocomposite modified with ZnO-NPs and (E102) for optical and antibacterial applications. Int J Biol Macromol. 2017;97:561-567.
22. Ghaedi M, Khajesharifi H, Hemmati Yadkuri A, Roosta M, Sahraei R, Daneshfar A. Cadmium hydroxide nanowire loaded on activated carbon as efficient adsorbent for removal of Bromocresol Green. Spectrochimica Acta Part A: Molecular and Biomolecular Spectroscopy. 2012;86:62-68.
23. Ikram M, Chaudhary K, Shahzadi A, Haider A, Shahzadi I, Ul-Hamid A, et al. Chitosan/starch-doped $MnO_2$ nanocomposite served as dye degradation, bacterial activity, and insilico molecular docking study. Materials Today Nano. 2022;20:100271.
24. Abureesh MA, Oladipo AA, Mizwari ZM, Berksel E. Engineered mixed oxide-based polymeric composites for enhanced antimicrobial activity and sustained release of antiretroviral drug. Int J Biol Macromol. 2018;116:417-425.
25. Bahramzadeh E, Yilmaz E, Adali T. Chitosan-graft-poly(N-hydroxy ethyl acrylamide) copolymers: Synthesis, characterization and preliminary blood compatibility in vitro. Int J Biol Macromol. 2019;123:1257-1266.
26. Alqahtani FY, Aleanizy FS, Tahir EE, Alquadeib BT, Alsarra IA, Alanazi JS, et al. Preparation, characterization, and antibacterial activity of diclofenac-loaded chitosan nanoparticles. Saudi pharmaceutical journal : SPJ : the official publication of the Saudi Pharmaceutical Society. 2019;27(1):82-87.
27. Ikram M, Shujait S, Haider A, Kashaf Ul A, Ul-Hamid A, Haider J, et al. Molybdenum and chitosan-doped MnO2 nanostructures used as dye degrader and antibacterial agent. Applied Nanoscience. 2022;12(12):3909-3924.
28. Dinh V-P, Le N-C, Tuyen LA, Hung NQ, Nguyen V-D, Nguyen N-T. Insight into adsorption mechanism of lead(II) from aqueous solution by chitosan loaded $MnO_2$ nanoparticles. Materials Chemistry and Physics. 2018;207:294-302.
29. Yadav M, Rhee KY, Park SJ, Hui D. Mechanical properties of $Fe_3O_4$/GO/chitosan composites. Composites Part B: Engineering. 2014;66:89-96.
30. Publisher Profile: IGI Global. Against the Grain. 2012;24(2).
31. Hassan SE-D, Fouda A, Saied E, Farag MMS, Eid AM, Barghoth MG, et al. Rhizopus oryzae-Mediated Green Synthesis of Magnesium Oxide Nanoparticles (MgO-NPs): A Promising Tool for Antimicrobial, Mosquitocidal Action, and Tanning Effluent Treatment. Journal of fungi (Basel, Switzerland). 2021;7(5):372.
32. Das S, Behera SS, Murmu BM, Mohapatra RK, Mandal D, Samantray R, et al. Extraction of scandium(III) from acidic solutions using organo-phosphoric acid reagents: A comparative study. Sep Purif Technol. 2018;202:248-258.
33. Zhang F, Chen X, Wu F, Ji Y. High adsorption capability and selectivity of ZnO nanoparticles for dye removal. Colloids Surf Physicochem Eng Aspects. 2016;509:474-483.
34. Emembolu LN, Ohale PE, Onu CE, Ohale NJ. Comparison of RSM and ANFIS modeling techniques in corrosion inhibition studies of Aspilia Africana leaf extract on mild steel and aluminium metal in acidic medium. Applied Surface Science Advances. 2022;11:100316.
35. Chijioke Elijah O, Nonso Collins O, Callistus Obumneme O, Jessica N-B. Application of Modified Agricultural Waste in the Adsorption of Bromocresol Green Dye. Asian Journal of Chemical Sciences. 2020:15-24.
36. Theydan SK. Effect of Process Variables, Adsorption Kinetics and Equilibrium Studies of Hexavalent Chromium Removal from Aqueous Solution by Date Seeds and its Activated Carbon by $ZnCl_2$. Iraqi Journal of Chemical and Petroleum Engineering. 2018;19(1):1-12.
37. Graphical Abstract: Angew. Chem. Int. Ed. 48/2014. Angew Chem Int Ed. 2014;53(48):12977-12992.
38. Arabkhani P, Asfaram A. Development of a novel three-dimensional magnetic polymer aerogel as an efficient adsorbent for malachite green removal. J Hazard Mater. 2020;384:121394.
39. Asadu CO, Anthony EC, Elijah OC, Ike IS, Onoghwarite OE, Okwudili UE. Development of an adsorbent for the remediation of crude oil polluted water using stearic acid grafted coconut husk (Cocos nucifera) composite. Applied Surface Science Advances. 2021;6:100179.
40. Onu CE, Ekwueme BN, Ohale PE, Onu CP, Asadu CO, Obi CC, et al. Decolourization of bromocresol green dye solution by acid functionalized rice husk: Artificial intelligence modeling, GA optimization, and adsorption studies. Journal of Hazardous Materials Advances. 2023;9:100224.
41. Liu D, Yuan J, Li J, Zhang G. Preparation of Chitosan Poly(methacrylate) Composites for Adsorption of Bromocresol Green. ACS omega. 2019;4(7):12680-12686.
42. Elwakeel KZ, El-Bindary AA, El-Sonbati AZ, Hawas AR. Magnetic alginate beads with high basic dye removal potential and excellent regeneration ability. Canadian Journal of Chemistry. 2017;95(8):807-815.